Soil Biology and Biochemistry 214 (2026) 110068

Contents lists available at ScienceDirect

Soil Biology and Biochemistry

journal homepage: www.elsevier.com/locate/soilbio

Enhanced methanogenesis in acidic fen peatlands via ferrihydrite reduction-driven microbial metabolisms

Hong-Yan Wang [a,b], Xin-Yi Hu [a], Feng-Wu Zhou [c], Julio-Castillo Hernandez [d], Zhi-Guo Yu [a,*], Maxim Dorodnikov [e], Klaus-Holger Knorr [e], Andreas Kappler [f]

[a] Key Laboratory Carbon Source and Sink-China of Ecosystem Meteorological Administration (ECSS-CMA)/School of Hydrology and Water Resources, Nanjing University of Information Science and Technology, Nanjing, China
[b] State Key Lab of Urban and Regional Ecology, Research Center for Eco-Environmental Sciences, Chinese Academy of Sciences, Beijing, 100085, China
[c] Department of Environmental Science and Engineering, Fudan University, Shanghai, China
[d] Department of Microbiology and Biochemistry, University of the Free State, Bloemfontein, South Africa
[e] University of Münster, Institute for Landscape Ecology, Ecohydrology and Biogeochemistry Group, Heisenbergstr. 2, Münster, 48149, Germany
[f] Geomicrobiology, Department of Geosciences, Tübingen, 72076, Germany

ARTICLE INFO

Keywords:
Acidic fen
Fermentative ferrihydrite reduction
Biomineralization
Organic matter decomposition
Methanogenesis
Metagenome-assembled genomes

ABSTRACT

Interactions between Fe(III) reduction and methanogenesis in regulating CH_4 emissions remain controversial, particularly in peatlands. To address this, we investigated the effects of ferrihydrite amendments on net CH_4 formation in four moderately acidic fen soils from the Great Khingan Mountains, the Changbai Mountains, the Tibetan Plateau, and Dajiuhu. Anaerobic microcosms were established to monitor gas formation and porewater chemistry, while detailed geochemical and microbiome profiling was conducted for the soils from the Changbai Mountains. Ferrihydrite additions increased net CH_4 formation rates by 1.4–6.2 times, with stronger effects observed in soils with more available carbon. As expected, secondary crystalline magnetite did not form. Ferrihydrite reduction mainly occurred during the pre-methanogenic stage and was mediated by fermentative Fe (III)-reducing bacteria, such as *Clostridium* and *OPB41*. These microbes lowered H_2 levels, reducing the relative abundance of *Methanobacterium* from 86% to 56%. However, fermentative Fe(III) reduction mitigated limitations on organic matter decomposition by elevating pH and improving the thermodynamic feasibility of organic carbon fermentation in the pre-methanogenic stage. Beyond enhanced substrate supply, the legacy of elevated pH further promoted activities of acetoclastic methanogens, as indicated by faster net acetate consumption in ferrihydrite treatments. Enriched metagenome-assembled genomes (MAGs) affiliated with *Sumerlaeaceae*, *Clostridium*, *OPB41*, and *Prolixibacteraceae* revealed the potential for polysaccharide hydrolysis and acetogenesis. Most of the enriched acetogens engaged in syntrophic interactions with methanogens. Collectively, our findings suggest that fermentative Fe(III) reduction can stimulate organic matter decomposition, while its legacy of elevated pH further accelerates organic matter decomposition and methanogenesis in acidic peatland soils.

1. Introduction

Peatlands cover only 3% of Earth's land surface but store nearly one-third of global soil carbon, thereby playing a critical role in the global carbon cycle. Nevertheless, prevailing anoxic conditions in the waterlogged peat make them a major natural source of methane (CH_4), with northern peatlands alone emitting up to ~36 CH_4–C Tg per year into the atmosphere (Fletcher et al., 2004; Chen and Prinn, 2006; Zhuang et al., 2006). CH_4 emissions in peatlands are strongly influenced by hydrology (Strack et al., 2004; Cui et al., 2024), geochemistry (Andersen et al., 2013), and microbial communities (Lin et al., 2014; Bräuer et al., 2020). Regeneration of electron acceptors, such as ferric iron, following water table drawdown is proposed to be a key factor influencing methane (CH_4) emissions (Knorr et al., 2009; Knorr and Blodau, 2009).

Methanogenesis from plant debris in anoxic environments is catalyzed by a syntrophic association among fungi, anaerobic bacteria and methanogenic archaea (Thauer et al., 2008; Conrad, 2020). Plant polymers are first hydrolyzed into monomers such as glucose, which are

* Corresponding author.
E-mail address: zhiguo.yu@nuist.edu.cn (Z.-G. Yu).

https://doi.org/10.1016/j.soilbio.2025.110068
Received 1 August 2025; Received in revised form 8 December 2025; Accepted 10 December 2025
Available online 11 December 2025

further fermented to produce methanogenic substrates including H_2, acetate, CO_2, and short-chain fatty acids (e.g. propionate and butyrate). These fatty acids serve as important intermediates for syntrophic methanogenic consortia that can also include Fe(III)-reducers (Drake et al., 2009). Hydrogenotrophic methanogenesis involves the reduction of CO_2 to CH_4 via interspecies electron transfer using H_2 or formate, whereas acetoclastic methanogenesis entails the disproportionation of acetate into CH_4 and CO_2. The balance between these two pathways is influenced by the substrate availability and methanogenic activity. Notably, proton concentration (pH) has been recognized as a critical environmental parameter regulating the predominance of either pathway in acidic peatlands (Kotsyurbenko et al., 2007; Ye et al., 2012).

In terrestrial environments, iron(III)-reducing bacteria are classified into two main groups: respiratory and fermentative types (Dong et al., 2017), which direct carbon into distinct metabolic pathways. Respiratory Fe(III)-reducers fully oxidize organic substrates, such as acetate, to CO_2 for energy conservation. The *Geobacteraceae* is considered a dominant group of respiratory Fe(III)-reducers in subsurface environments (Lin et al., 2009). In contrast, fermentative Fe(III)-reducers utilize Fe(III) primarily as an electron sink to dispose of excess reducing equivalents, thereby enhancing fermentation efficiency (Lovley et al., 2004; Lehours et al., 2010; List et al., 2019). Emerging evidence also suggests that fermentative Fe(III) reduction may enhance organic matter fermentations by buffering system acidification (Dong et al., 2017; Zhang et al., 2023).

Respiratory iron(III) reduction is more thermodynamically favorable than methanogenesis, enabling Fe(III)-reducers to outcompete methanogens for substrates such as H_2 and acetate. This competition has been proven to inhibit CH_4 formation in paddy soils (Luo et al., 2023), marine sediments (Bray et al., 2017) and permafrost soils (Voggenreiter et al., 2025a). However, some studies have found co-existence of methanogenesis and Fe(III) reduction (Bethke et al., 2011; Yang et al., 2016; Marquart et al., 2019; Vigderovich et al., 2019; Aromokeye et al., 2021). In some cases, the Fe(III) reduction even stimulates methanogenesis (Zhuang et al., 2015; De Jong et al., 2020). For example, in anoxic environments, dissolved Fe(II) can promote recrystallization of Fe(III) (oxyhydr)oxides to more thermodynamically stable phases such as magnetite (Fe_3O_4) (Yang et al., 2010; Jones et al., 2017). Formation of magnetite has been shown to enhance methanogenesis by facilitating interspecies electron transfer (Zhuang et al., 2015; Giangeri et al., 2023). De Jong et al. (2020) propose that the formation of magnetite via ferrihydrite biomineralization in peatlands facilitates methanogenesis, though direct evidence for this is lacking. Additionally, it has also been suggested that Fe(III) reduction leads to an increase in pH in acidic peat soils, creating conditions that are more favorable for acetoclastic methanogenesis (Sulman et al., 2022). However, this hypothesis remains unverified in the absence of comprehensive geochemical and microbial investigations. Given these contradictory findings and the complexity of underlying mechanisms, a detailed investigation is needed to understand how Fe(III) reduction drives geochemical changes and alters microbial trophic interactions in acidic peatlands.

We hypothesize that magnetite formation is unlikely in organic carbon-rich peat soils due to formation of organic matter–Fe(II) complexes or precipitates. Furthermore, Fe(III) reduction may only weakly compete with methanogenesis for common substrates, yet promote organic matter decomposition and CH_4 formation by altering geochemical conditions. To test these hypotheses, peat soils were collected from four sites in China representing acidic poor fens. Among these, peatlands in the Great Khingan Mountains (TQ) and on the Tibetan Plateau (HY) exhibit a lesser degree of decomposition compared to those in the Changbai Mountains (DT) and Dajiuhu (DJH). Anoxic incubation experiments were conducted both with and without the addition of ferrihydrite. Preliminary results showed that ferrihydrite reduction consistently stimulated methanogenesis across all peat soils, accompanied by similar changes in porewater chemistry and gas profiles. Given the variation in parameters among sites, the DT peat was selected for in-depth geochemical and microbiome analyses as the most balanced to investigate potential competition and synergistic interactions between ferrihydrite reduction and methanogenesis. In summary, the objectives of this study were to (1) investigate the influence of microbial ferrihydrite reduction on methanogenesis in acidic peat soils; (2) characterize geochemical changes, including porewater chemistry, methanogenic substrates and ferrihydrite biomineralization; and (3) elucidate responses of microbial communities and metabolic potentials to ferrihydrite reduction and their regulatory roles in net CH_4 formation.

2. Materials and methods

2.1. Peat soil collection and preparations

We collected peat soils from four representative peatlands across different climatic zones in China (Fig. S1): Dongtu (DT) in the Changbai Mountains, Tuqiang (TQ) in the Greater Khingan Mountains, Dajiuhu (DJH), and Hongyuan (HY) in the Zoige Plateau, Tibet. These peatlands are primarily rain-fed, with vegetation dominated by vascular plants such as *Carex* spp., along with minor contributions from mosses. Based on the vegetation composition and porewater pH (~5.0–~5.5), these peatlands are classified as poor acidic oligotrophic fens (Watmough et al., 2022). Additional information about the studied peatlands can be found elsewhere (Liu et al., 2019; Song et al., 2021; Zhang et al., 2022; Wang et al., 2024).

Six peat cores (5 cm in diameter) were randomly collected from the top 30 cm using a Russian peat corer (Eijkelkamp Agrisearch Equipment, the Netherlands), with subsamples taken within a 5.0 m diameter area. The cores were sealed in sterile sampling bags, transported to the laboratory on ice, and stored at 4 °C (less than six months) until incubations. Peat from the 10–30 cm depth was chosen for incubation because this layer was water-saturated during field sampling, which inhibited aeration by atmospheric oxygen. The humification degree of peat soils was assessed using the von Post index based on parameters including color, recognizable plant fiber remains, and water release (Riley and Michaud, 1994). Before incubations, samples from each site were thoroughly homogenized, and visible plant debris and roots were removed. The peat was then air-dried and ground using a tungsten carbide mill (Retsch MM400, Haan, Germany).

Carbon (C) and nitrogen (N) contents in peat soils were measured using an elemental analyzer (UNICUBE, Germany). Iron (Fe) was extracted with 2 mol L^{-1} hydrochloric acid (HCl) at a soil-to-water ratio of 1:200 (w:v) for 24 h, and its concentration was determined using the ferrozine assay (Viollier et al., 2000). Water-extractable organic carbon (WEOC) was obtained by shaking air-dried peat with ultrapure water at a 1:10 (w:v) ratio for 12 h. The suspension was then filtered through 0.45-μm nylon filters, and the supernatant was acidified to pH < 2 using phosphoric acid (H_3PO_4). The WEOC concentrations were measured using a TOC analyzer (TOC-L, Shimadzu, Japan). Specific ultraviolet absorbance at 254 nm ($SUVA_{254}$) was calculated by dividing the absorbance at 254 nm (A254, m^{-1}) by the WEOC concentration (mg L^{-1}) (Weishaar et al., 2003), providing an indicator of the organic matter aromaticity (Chin et al., 1994). Lignin phenols in peat soils were extracted using the CuO oxidation method and subsequently analyzed by a gas chromatography–mass spectrometry (GC-MS, Thermo Fisher Scientific, USA) equipped with a DB-5 MS capillary column (Wang et al., 2017).

2.2. Incubation treatments

The experimental design included five treatments for each of the four peat soils: (1) Control – peat soil only; (2) Fh – peat with ferrihydrite; (3) AQDS – peat with anthraquinone-2,6-disulfonate (AQDS); (4) Fh+AQDS – peat with ferrihydrite and AQDS; (5) Fh+BES – peat with ferrihydrite and 2-bromoethanesulfonate (BES). The AQDS at 200 μmol L^{-1} was used as an electron shuttle to promote ferrihydrite reduction (Lovley et al.,

1996; Nevin and Lovley, 2002), whereas BES at 40 mmol L^{-1} served as a methanogenesis inhibitor to assess syntrophic interactions between bacteria and methanogens in the presence of ferrihydrite (Zhang et al., 2020; Yang et al., 2021).

All incubation and sampling were conducted inside a glovebox (Mikrouna, Shanghai) under a N_2 atmosphere (100% N_2, $O_2 < 1$ ppm). Ferrihydrite was synthesized according to Schwertmann and Cornell (2000) by neutralizing 0.4 mol L^{-1} ferric chloride ($FeCl_3$) with 1 mol L^{-1} NaOH until the suspension reached pH ≈ 7.0, after which the precipitate was dialyzed to remove residual salts. X-ray diffraction (XRD) analysis confirmed the formation of two-line ferrihydrite (Fig. S2). For each incubation, 2.0 g (dry weight) of milled peat and 0.2 g of fresh peat (0.02 g dry weight) were added to 250 mL serum bottles containing 100 mL of deionized water. Ferrihydrite was added to achieve the Fe(III) concentration of ~10 mmol L^{-1}, equivalent to ~570 μmol g^{-1} dry peat, as confirmed by acid extractions. Incubation treatments including Control, Fh, AQDS, Fh+AQDS, and Fh+BES were prepared in triplicate. The Fh+BES treatment was amended with BES at the onset of quantitative CH_4 formation to inhibit methanogenic activities (Zhang et al., 2020; Yang et al., 2021). Serum bottles were sealed with butyl-rubber stoppers (Glasgerätebau Ochs, Bovenden, Germany) and purged with pure N_2 for 90 min to ensure anoxic conditions. All incubations were processed at 25 °C in the dark. Solute chemistry and net gas formation were monitored by periodic sampling of aqueous and headspace gases, respectively.

2.3. Solute chemistry and gas analysis

Solute samples were collected from peat suspensions using a hypodermic needle and filtered through 0.45 μm nylon membranes. Total dissolved Fe was measured at 562 nm using a spectrophotometer (DR6000, Hach, Loveland, CO, USA) following the ferrozine method (Viollier et al., 2000). In this method, Fe(III) was reduced to Fe(II) using hydroxylamine hydrochloride. The pH was measured with a pH electrode (SenTix and ProfiLine 3310, WTW, Germany).

At each sampling point, 2.0 mL of headspace gas was collected using a sterile syringe. The concentrations of CH_4, CO_2 and H_2 were determined using a gas chromatograph (GC8090B, Agilent, USA) equipped with both a flame ionization detector (FID) and a thermal conductivity detector (TCD). The H_2 was quantified by TCD throughout the incubations, with a detection limit of ~10 ppm. The CH_4 and CO_2 concentrations were measured using FID when below 2000 ppm, and TCD when exceeding this threshold. Aqueous concentrations of CH_4, CO_2 and H_2 were calculated from headspace values using Henry's law and solute pH values (Stumm and Morgan, 1996). After each sampling, 2.0 mL of N_2 was replenished into bottles. Cumulative contents of CH_4, CO_2 and H_2 were normalized to μmol g^{-1} dry peat.

Separately for the DT peat soil, DOC concentration was measured by a TOC analyzer (TOC-L, Shimadzu, Japan), due to interference from AQDS and BES, the DOC concentration was only analyzed in the Control and ferrihydrite-amended treatment. Low-molecular-weight organic acids were selectively analyzed in the Control, Fh, and Fh+AQDS treatments using high-performance liquid chromatography (HPLC; SPD-M20A, Shimadzu) to assess the organic matter decomposition under ferrihydrite addition. To investigate shifts in methanogenic pathways induced by ferrihydrite addition, the carbon isotopic compositions ($\delta^{13}C$) of CH_4 and CO_2 were analyzed in the Control and Fh treatments at the end of methanogenesis stage, complementing the microbial analyses. The measurement was conducted by an isotope ratio MS (Delta V advantages, thermos, Germany). The carbon isotope fractionation factor (α_c) was calculated from carbon isotope composition of CH_4 ($\delta^{13}C_{CH4}$) and CO_2 ($\delta^{13}C_{CO2}$) (Conrad, 2005):

$$\alpha_c = (\delta^{13}C_{CO2} + 10^3)/(\delta^{13}C_{CH4} + 10^3)$$

2.4. Fe speciation in solid phase

Ferrihydrite biomineralization in the DT peat soil was characterized at the end of the incubation using selective extraction methods (Coward et al., 2017). The extraction was performed inside the glovebox once the peat soil had been dried. Two chemical extraction protocols were applied to quantify distinct iron phases: (1) "amorphous/poorly crystalline Fe (oxyhydr)oxides" (e.g. ferrihydrite), extracted with 0.25 mol L^{-1} HCl hydroxylamine; and (2) "crystalline Fe oxides" (e.g. goethite and magnetite), extracted using citrate-bicarbonate-dithionite (CBD) (Yang et al., 2022). For each extraction, 0.2 g of peat soil was placed into a 50 mL centrifuge tube with 20 mL of the extractant. After shaking in the dark for ~16 h, the supernatants were decanted, filtered through 0.45 μm nylon membrane filters, and transferred to 50 mL tubes for Fe concentration analysis. Additionally, reactive Fe phases including ferrihydrite and less crystalline Fe forms were extracted using 2 mol L^{-1} HCl to determine contributions of Fe(II) and Fe(III) (Wang et al., 2020). For this extraction, ~0.1 g of soil was mixed with 20 mL of HCl, shaken for 20 h, and then filtered through 0.45 μm nylon filters. Concentrations of Fe(II) and Fe(III) in the filtrates were measured using the ferrozine assay.

2.5. DNA extraction and quantitative real-time PCR (qPCR)

After finishing the incubation, DT peat soils from the Control, Fh, Fh+BES, and Fh+AQDS treatments were stored at −80 °C prior to DNA extraction. DNA was extracted from each sample in triplicate using the PowerSoil™ DNA Isolation Kit (Invitrogen, USA) according to the manufacturer's protocol. DNA concentration was measured using a Nanodrop spectrophotometer (ND-1000, USA).

The qPCR was conducted in triplicate to quantify 16S rRNA genes of bacteria, archaea, *Geobacteraceae*, as well as the methyl-coenzyme M reductase subunit alpha (*mcrA*) gene. Primers used were: Bac341F (forward) and Bac806R (reverse) for bacteria; Arch524F (forward) and Arch958R (reverse) for archaea; 577F (forward) and 822R (reverse) for *Geobacteraceae*; and ME1F (forward) and ME2R (reverse) for *mcrA* gene. Details of primer sequences, reaction mixtures, and thermal cycling conditions are provided in the Supporting **text** and Table S1. Standard curves were generated using a 10-fold serial dilution of plasmid DNA, ranging from 10^2 to 10^8 gene copies per reaction. Final gene copy numbers were normalized per gram of dry peat soil.

2.6. Bacterial and archaeal 16S rRNA gene sequencing and data analysis

Same primers used in qPCR were applied for 16S rRNA gene sequencing of bacteria and archaea. Details of PCR reaction mixtures and thermal cycling conditions are provided in the Supporting **information**. PCR amplicons were purified, quantified, pooled, and sequenced on an Illumina MiSeq PE 250 platform (BIOZERON Biotechnology Co., Ltd., Shanghai, China).

Raw data were demultiplexed, and quality-filtered using QIIME2. Reads with an average quality score below 20 over a 10 bp sliding window, lengths under 50bp, barcode mismatches, or ambiguous bases were removed. Low-quality sequences (quality score < 35) and chimeras were identified and filtered out before downstream analysis by DADA2 (Callahan et al., 2016). Finally, each ASV was classified using the SILVA (SSU138.1) 16S rRNA database with a confidence threshold of 97%.

2.7. Metagenomic sequencing and data analysis

To assess differences in carbon degradation potential and the functional capacities of microbes enriched by ferrihydrite, metagenomic sequencing was performed on both the Control and Fh treatment of DT peat soil. Genomic DNA from the Control and Fh was subjected to metagenomic analysis. A total of six samples were sequenced, generating approximately 120 Gb of raw data.

Paired-end raw reads were de-replicated and trimmed using "fastp" (v0.20.0) with parameters of -D, -q 20 and -l 50. The assemblies were generated using SPAdes (v4.0) with a minimum contig length of 500 bp (Chen, 2023). Open reading frames (ORFs) were predicted from assembled contigs using Prodigal (Hyatt et al., 2012). ORFs were clustered using CD-HIT (95% sequence identity and 90% coverage), and the longest sequence of each cluster was selected to construct a non-redundant gene catalog. Taxonomic annotations were assigned by aligning the gene catalog to NCBI NR database using BLAST (e-value: 0.00001) (Pruitt et al., 2012). Annotation of functional genes was conducted using kofamscan (v1.2.0) against KEGG database (Aramaki et al., 2020). Additionally, contigs were screened for carbohydrate-active enzymes (CAZyme) using CAZy database with HMMscan and default settings. Gene abundances were quantified using Salmon software (v.0.7.2) and converted into transcripts per million mapped counts (TPM) (Patro et al., 2017).

Contig co-assemblies were binned using metaWRAP (Uritskiy et al., 2018), and metagenome-assembled genomes (MAGs) were initially filtered with MDMcleaner (v0.8.7). The MAG contamination and completeness were evaluated using CheckM (v1.0.11), and dereplication was performed at 99% average nucleotide identity using dRep (v3.4.0). MAGs with ≥75% completeness and ≤10% contamination were retained for further analysis. Taxonomic assignment was done using GTDB-Tk. Genes in MAGs were predicted with PROKKA (default settings), and functional annotations were mapped against the KEGG database (Seemann, 2014). Functional gene abundance was calculated as transcripts per million (TPM).

2.8. Statistical analysis

Statistical analysis was performed using SPSS (IBM SPSS Statistics, v26.0). Differences in peat chemical properties were analyzed using one-way ANOVA. To evaluate differences in net CH_4 formation rates during the methanogenic phase, a two-way ANOVA was performed to examine the effects of peat site and treatment (Control, AQDS, Fh, Fh+AQDS) and their interactions. In the methanogenic phase, one-way ANOVA was employed to assess significant differences among treatments within each peat soil.

2.9. Data availability

Raw shotgun metagenome gene and 16S rRNA sequences from this study are available in the NCBI Sequence Read Archive under the accession number PRJNA1132364.

3. Results

3.1. Physiochemical properties of peat soils

Humification indices of collected peat soils according to von Post scale ranged from H5 to H7, while the C/N ratio was below 20 (Table 1). The soils exhibited acidic properties, with pH values ranging from 4.6 to 5.1. Compared to TQ and HY, DT and DJH exhibited lower C/N ratios, whereas WEOC contained higher levels of aromatic compounds. Lignin phenol concentrations varied from 1.5 to 4.7 g kg^{-1} peat, with notably lower levels observed at DJH. The Fe content extracted using 2 M HCl ranged from 66 to 153 μmol g^{-1} peat.

3.2. Greenhouse gas dynamics and geochemistry

3.2.1. Net CH_4 and CO_2 formation

During the pre-methanogenic phase (S1), the rate of methanogenesis was consistently low, averaging 0.5 ± 0.4 μmol g^{-1} d^{-1} (Fig. 1AF). Following S1, methanogenesis initiated much more rapidly in the Fh treatment. In the Fh and Fh+AQDS treatments, the net CH_4 formation increased linearly from approximately days 20–30 in DT, HY, and TQ, and from day 40 in DJH (Fig. 1AF). We defined the period of linear increase in the Fh+AQDS and Fh treatments as the methanogenic phase (S2).

Two-way ANOVA indicated that treatments, peat sites, and their interactions significantly affected net CH_4 formation rates ($P < 0.001$, Table S2) in S2. In the Fh treatment, methanogenesis rates ranged from 3.2 to 15.5 μmol g^{-1} d^{-1} across peat soils, approximately 1.5–6.2 times higher than in the Control. AQDS addition further increased net CH_4 formation rate in TQ peat soil. Both the Fh and Fh+AQDS treatments in TQ and HY soils produced significantly higher cumulative CH_4 than those in the DT and DJH soils, which was associated with lower aromaticity indices. Similarly, ferrihydrite stimulated CH_4 formation rates more strongly in TQ and HY compared to DT and DJH. In line with these patterns, cumulative CO_2 content was also higher in the Fh and Fh+AQDS treatments of TQ and HY soils (Fig. 1B). However, ferrihydrite did not significantly influence net CO_2 formation during S1.

3.2.2. Ferrihydrite reduction

Ferrihydrite reduction proceeded rapidly during the S1, as evidenced by the sharp increase in dissolved Fe concentration (Fig. 1C). In the Fh treatment, the Fe concentration in solution increased from 0.7 to 1.3 μmol g^{-1} d^{-1} across peat soils, reaching an average of 29 ± 9 μmol g^{-1} by the end of S1. The addition of AQDS further enhanced ferrihydrite reduction, elevating Fe release rates to 1.7–2.2 μmol g^{-1} d^{-1}. During the S2 phase, net Fe release dropped significantly in the Fh treatment and stopped entirely in TQ. It also ceased under the Fh+AQDS treatment in most peat soils. When methanogenesis was inhibited by BES, a concurrent increase in solution Fe was also observed.

3.2.3. The net H_2 formation

The H_2 level peaked at the beginning of incubation in all treatments, then decreased and stabilized at less than 0.1 μmol g^{-1} peat (less than 40 nmol L^{-1} in solution) (Fig. 1D). Coinciding with rapid ferrihydrite reduction in the S1, the H_2 level in the Fh treatments was consistently 1.6–4.3 μmol g^{-1} lower compared to the Control. The addition of AQDS further decreased H_2 concentrations by approximately 5.2–9.8 μmol g^{-1} peat relative to Control.

3.2.4. Solute pH value

The pH levels varied among different treatments across distinct methanogenic phases (Fig. 1E). In S1, pH in the Control was moderately acidic (4.4–5.0), while ferrihydrite additions significantly increased the

Table 1
Geochemical composition of peat soils used in incubations.

Site	C %	N %	C/N	H %	Lignin phenols g kg^{-1}	Fe μmol g^{-1}	pH	WEOC mg L^{-1}	$SUVA_{254}$ L mg^{-1} m^{-1}
TQ	38	2.2	17	5.9	3.9	153	4.6	546 ± 14^{d}	0.27 ± 0.05^{a}
HY	39	2.1	18	5.8	4.7	66	4.7	371 ± 12^{b}	0.31 ± 0.01^{a}
DJH	26	1.7	15	4.4	1.5	148	5.1	300 ± 7.8^{a}	0.57 ± 0.03^{b}
DT	34	2.4	14	5.5	4.3	91	5.1	402 ± 5.6^{c}	0.51 ± 0.07^{b}

WEOC: water-extractable organic carbon concentration, the C/N demonstrated mass ratio of carbon to nitrogen, $SUVA_{254}$: specific ultraviolet absorbance at 254 nm ($SUVA_{254}$). Different lowercase letters indicate significant differences. TQ, Tuqiang in the Greater Khingan Mountains; HY, Hongyuan in Zoige Plateau, Tibet; DJH, Dajiuhu peatland; DT, Dongtu (DT) in the Changbai Mountains. Different letters assigned to WEOC and $SUVA_{254}$ indicate significant differences among sites.

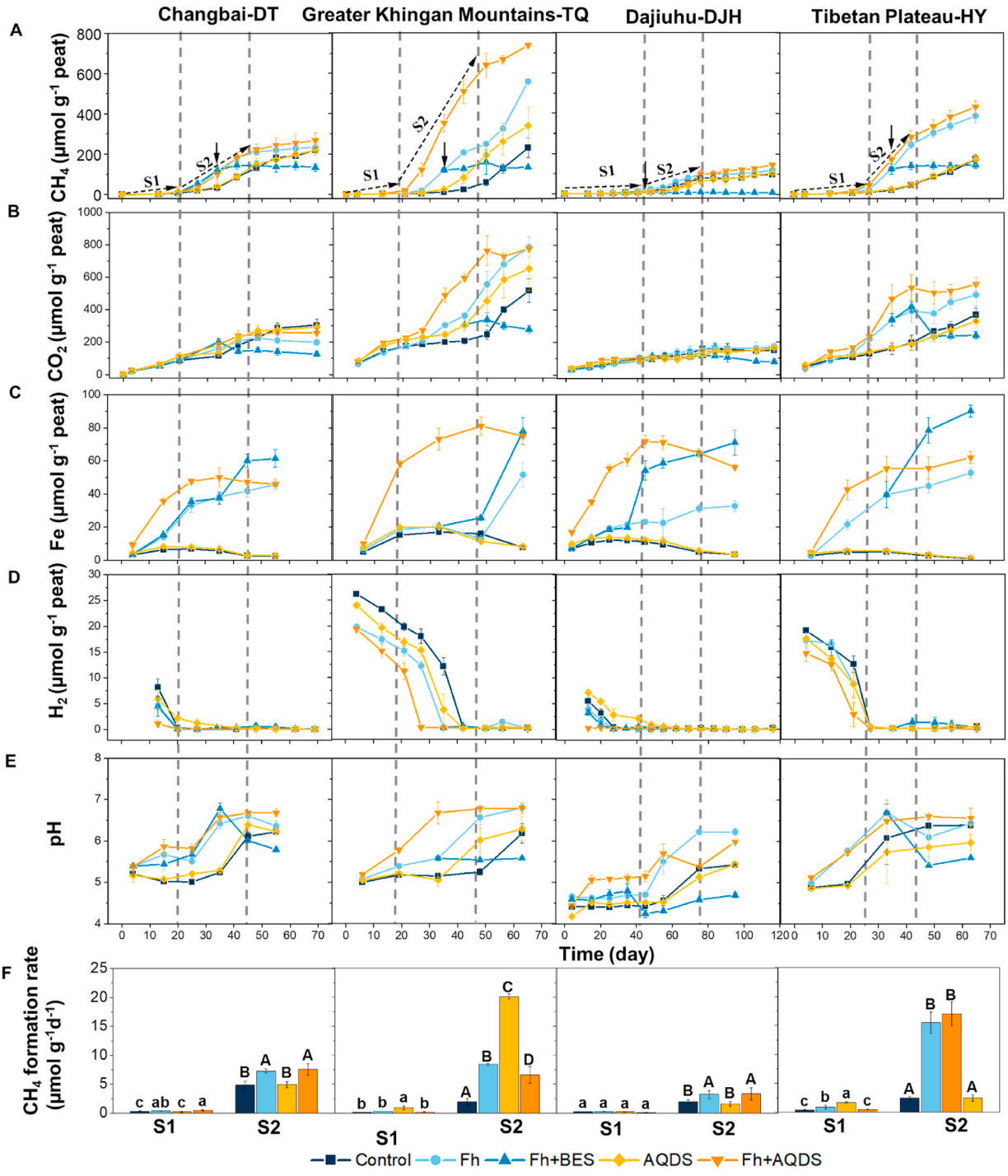

Fig. 1. Dynamics of **(A)** net CH_4 formation, **(B)** net CO_2 formation, **(C)** dissolved Fe concentrations, **(D)** net H_2 formation, **(E)** solute pH, and **(F)** net CH_4 formation rate under different experimental treatments. S1: pre-methanogenic phase; S2: methanogenic phase. Black arrows indicate the timing of 2-bromoethanesulfonate (BES) addition in Fh + BES treatment. Lowercase letters denote differences in net CH_4 formation rates among treatments within each peat soil type during S1, while uppercase letters indicate differences during S2 ($P < 0.01$ or $P < 0.05$).

pH by 0.2–0.7 units. In S2, the rapid net formation of CH_4 coincided with a fast rise in pH to above 6.0, except for the Control in the DJH soil. Overall, the Fh+AQDS and Fh treatments showed consistently higher pH values than the Control throughout S1 and S2. Furthermore, when BES was added, the solute pH decreased significantly in the Fh treatment.

3.3. Detailed geochemical characteristics in DT peat soil

3.3.1. The dynamics of dissolved organic carbon characteristics and isotopic compositions

By the end of S1, the DOC concentration in the Fh treatment was significantly higher than in the Control, at 110 mg L^{-1} versus 98 mg L^{-1} (Fig. 2a). Among all analyzed low-molecular-weight acids, acetate showed the highest concentrations (Fig. S3), ranging from ~1600 to ~2700 μmol L^{-1}. The acetate concentration in the Fh and Fh + AQDS

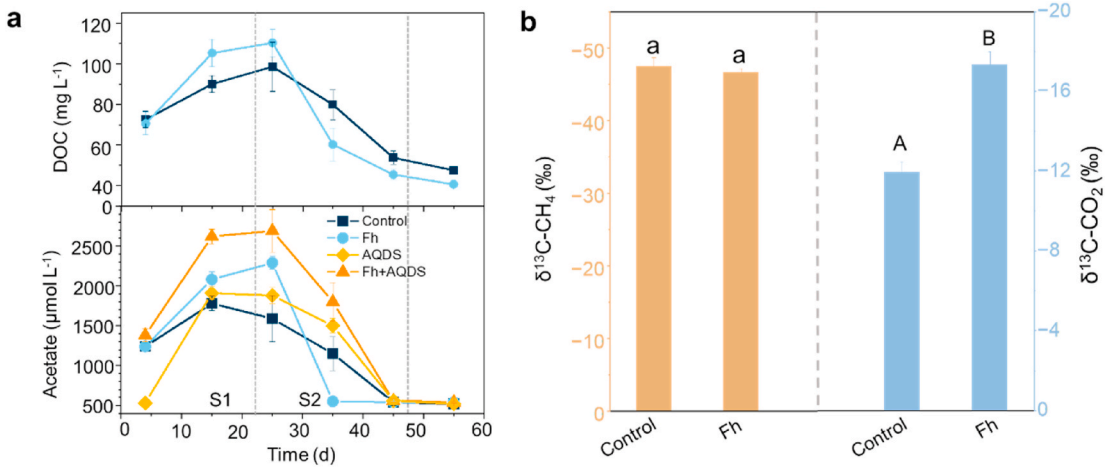

Fig. 2. Dynamics of dissolved organic carbon (DOC) characteristics **(a)** and isotopic compositions of CO_2 and CH_4 at the end of S2 **(b)** in different treatments of the Changbai-DT peat soil. S1: pre-methanogenic phase, S2: methanogenic phase. Lowercase letters in Fig. 2b indicate differences in $\delta^{13}C$ of CH_4 between control and Fh treatment, while uppercase letters indicate differences in $\delta^{13}C$ of CO_2.

treatments was 1.4 and 1.7 times higher than in Control, respectively (Fig. 2a). During the S2 methanogenic phase, the net acetate consumption rates were higher in the Fh and Fh + AQDS treatments compared to Control.

In the Control, the average $\delta^{13}C$ values of CH_4 and CO_2 were −47.4 ± 1.2‰ and −11.9 ± 0.4‰, respectively (Fig. 2b). Upon addition of ferrihydrite, the $\delta^{13}C$ of CO_2 decreased to −17.3 ± 0.7‰. The carbon fractionation factor (α_C) between CH_4 and CO_2 was approximately 1.037 in Control and 1.031 in the Fh treatment, consistent with the predominance of acetoclastic methanogenesis (Whiticar, 1999).

3.3.2. Biomineralization of ferrihydrite

Approximately one-third of the amended ferrihydrite was reduced to Fe(II) in the Fh treatment, while ferrihydrite was completely reduced in the presence of AQDS, as shown by 2 M HCl extractions (Fig. 3a, Table S3). Notably, in the Fh+BES treatment, all amended ferrihydrite was also reduced to Fe(II). The distribution of Fe(II) species between solution and peat soil indicated that up to 90% of Fe(II) was re-adsorbed onto peat soils. Comparable amounts of Fe were extracted using both HCl hydroxylamine and citrate-bicarbonate-dithionite (Fig. 3b, Table S3).

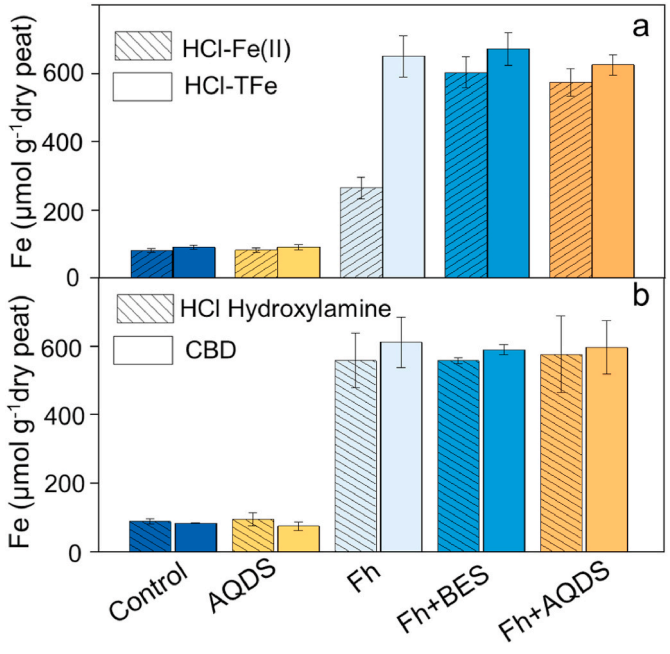

Fig. 3. Selective extractions for Fe speciation in DT peat soil at the end of the incubation period. **(a)** Content of Fe(II) and total Fe (TFe) in 2 M HCl extractions; **(b)** Selective extraction results with HCl Hydroxylamine and citrate-bicarbonate-dithionite (CBD).

3.4. Microbial composition and metabolic potential in response to ferrihydrite addition in DT peat soil

3.4.1. Quantification of bacteria, archaea, Geobacteraceae and mcrA

In the presence of ferrihydrite, bacterial 16S rRNA gene copy numbers increased by more than 2-fold, and the addition of AQDS further enhanced microbial abundance in both bacteria and archaea ($P < 0.01$) (Fig. 4A and B). In the Control, the *mcrA* gene copy number was quantified at 9.7 ± 0.1 10^6 g^{-1} peat, which decreased by ~6 times with ferrihydrite additions (Fig. 4C). Although ferrihydrite amendment increased the abundance of *Geobacteraceae* from 2.8 ± 0.2 10^3 to 9.9 ± 1.9 10^3 g^{-1} peat, this group accounted less than 0.001% of the total bacterial gene copies (Fig. 4D).

3.4.2. Bacterial and archaeal composition obtained from 16S rRNA gene sequencing

In Control, the bacterial community at the phylum level was dominated by *Bacillota* (33 ± 9.1%), *Pseudomonadota* (28 ± 4.0%), *Bacteriodota* (17 ± 2.6%), and *Acidobacteriota* (6.7 ± 2.6%), collectively accounting for over 80% of the total bacterial population (Fig. S4). In the Fh treatment, the relative abundance of *Clostridium* increased from 5.6 to 9.6% (Fig. S5a), while *OPB41* (formerly belonging to *Anaerosomatales*) increased 4-fold to comprise up to 14% of the bacterial population (Fig. 5a, data shown as Z-score). The relative abundance of *Prolixibacteraceae* and *Sumerlaeaceae* increased from 0.9% to 7.5%, and from 2.3% to 6.4%, respectively. Among archaea, the relative abundance of *Bathyarchaeia* increased from 28% in Control to 47% in the Fh treatment (Fig. 5b, data shown as Z-score). As expected, *Geobacteraceae* accounted for less than 1.0% in the Fh treatment. When methanogenesis was inhibited, the relative abundances of *Sumerlaeaceae*, *OPB41*, *Prolixibacteraceae*, and *Bathyarchaeia* all decreased simultaneously (Fig. 5a). Phylogenetic analysis revealed that most abundant 16S rRNA sequences in *OPB41* were closely related to another sediment isolate *Coriobacteriaceae bacterium strain Es71-Z0120* (Fig. S6).

The main methanogens detected were *Methanobacterium*, *Methanosarcina*, *Methanomassiliicoccus*, and *Methanocella* (Fig. 5b, Fig. S5b). Within the methanogenic community, the relative abundance of

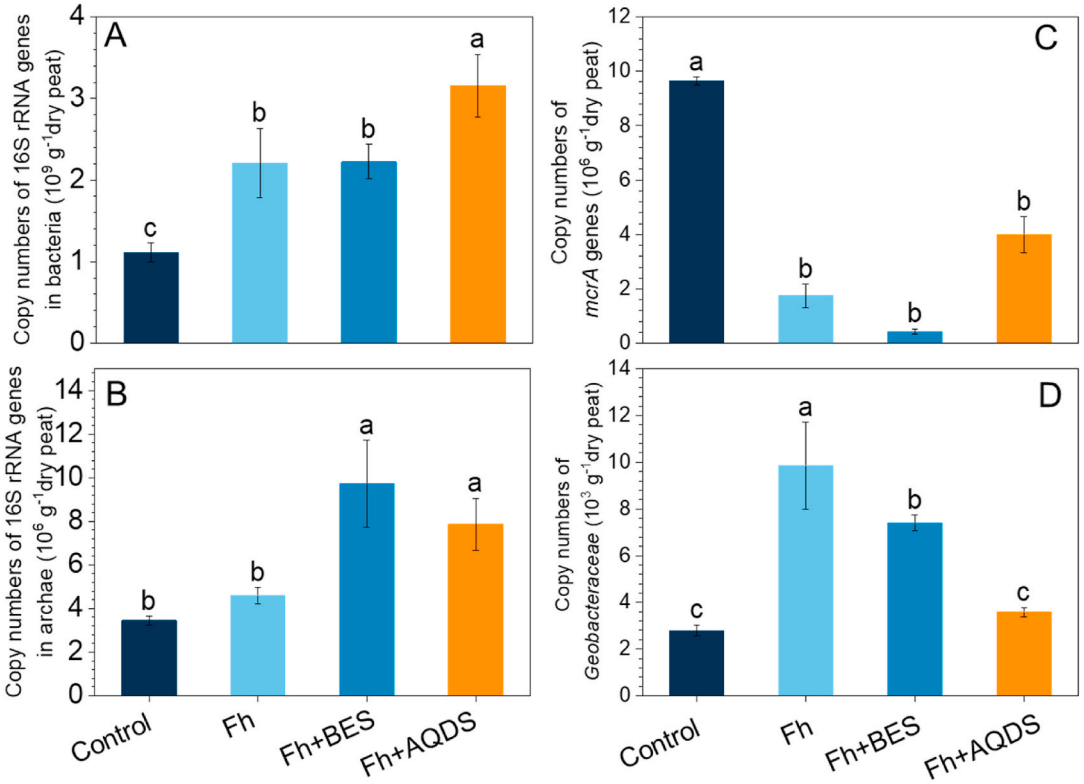

Fig. 4. Copy numbers of 16S rRNA genes of bacteria **(A)**, archaea **(B)**, the *mcrA* gene **(C)** and 16S rRNA genes of *Geobacteraceae* **(D)** in different experimental treatments. Different letters above the bars demonstrated significant differences in gene copy numbers ($P < 0.01$ or $P < 0.05$).

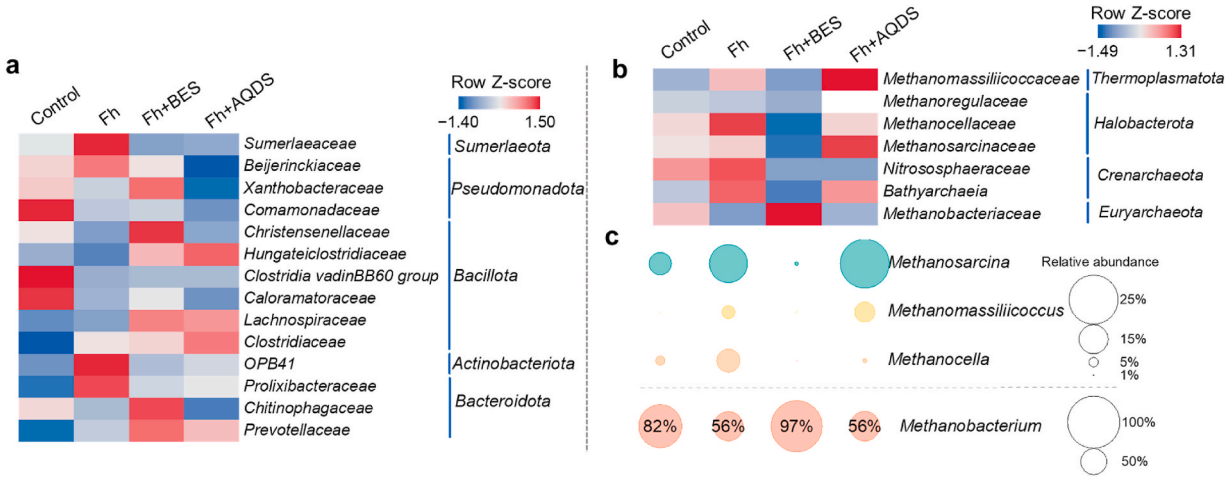

Fig. 5. Bacterial, archaeal and methanogenic compositions in different incubation treatments, as determined by 16S rRNA gene sequencing. **(a)** Heatmap showing relative abundance of main bacteria (>2%) at family level, scaled by row (Z-Score); **(b)** Heatmap showing relative abundances of archaea (>2%) at family level, scaled by row (Z-Score); **(c)** Bubble plot showing relative abundances of main methanogenic taxa within methanogen communities.

Methanobacterium decreased from 82% to 56% after ferrihydrite addition (Fig. 5c), whereas *Methanosarcina* increased from 11% in the Control to 19%, and further to 24% in the Fh+AQDS treatment. In addition, *Methanocella* and *Methanomassiliicoccus* also increased after ferrihydrite addition, from 5% to 11% and from <1% to 7%.

3.4.3. Metagenomics

Compared with the Control, key functional genes involved in the hydrolysis of celluloses and hemicelluloses (*uidA* [beta-glucuronidase], *gmuG* [mannan endo-1,4-beta-mannosidase], and *abfA* [alpha-L-arabinofuranosidase]), and other oligosaccharide degradation pathways (*xynB* [xylan 1,4-beta-xylosidase]) were significantly enriched ($P < 0.05$ or $P < 0.01$) in the Fh treatment (Fig. 6). Among the CAZyme families, relative abundances of glycoside hydrolases (GHs), auxiliary activities (AAs) and carbohydrate-binding modules (CBMs), all of which were involved in polysaccharide hydrolysis, were significantly higher in the Fh treatment compared to the Control (Fig. S7). Additionally, functional genes encoding pyruvate ferredoxin oxidoreductase (*porA*) and acetate kinase (*ackA*) were also significantly increased, indicating the enhanced potentials of fermentation and acetogenesis, respectively (Fig. 6).

A total of 319 MAGs were reconstructed from samples of both Control and Fh treatment (Fig. S8). Among them, 12 MAGs belong to

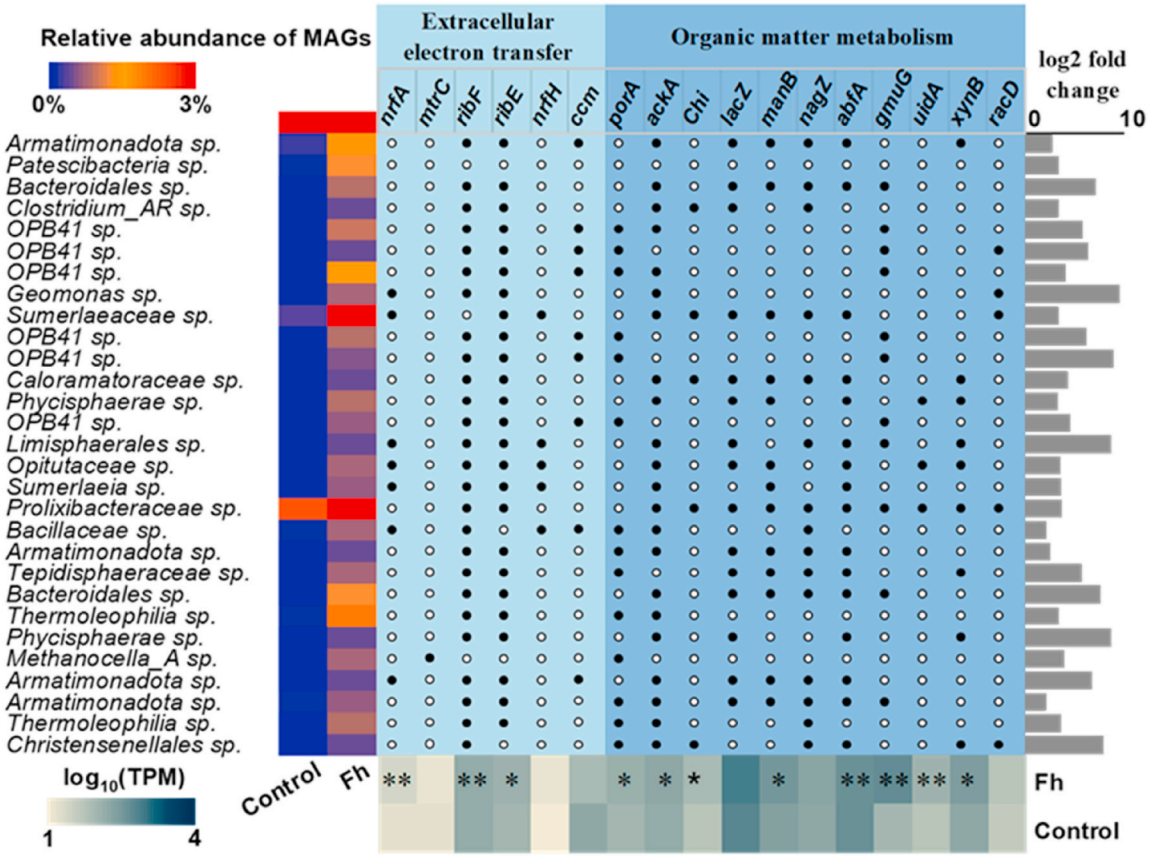

Fig. 6. Statistical analysis of selected functional genes in enriched metagenome-assembled genomes (MAGs) from ferrihydrite-amended (Fh) treatment compared to the control. Selective metabolic potentials in enriched MAGs of Fh (relative abundance >0.4%, log2 fold change >2) were profiled, the heatmap in columns demonstrates the relative abundance of MAGs in the control and Fh treatment. Presence/absence of genes in enriched MAGs of Fh is indicated by black/white dots. The heatmap in rows represents metabolic potentials in community levels, **: $P < 0.01$; *: $P < 0.05$. *chi*: abbreviations for Chitinase. Enzymes encoded by functional genes are described in Table S4.

Sumerlaeaceae, 13 MAGs belong to *OPB41*, 5 MAGs belong to *Clostridiaceae*, and 4 MAGs belong to *Prolixibacteraceae*. The main enriched MAGs from *Sumerlaeaceae* and *Prolixibacteraceae* encoded genes with potential for organic matter hydrolysis (e.g. hemicellulose) and acetogenesis (Fig. 6). The presence of *ribEF* genes (*ribE* [riboflavin synthase], *ribF* [riboflavin kinase]) in *Clostridium_AR* sp. suggests that extracellular electron transport in *Clostridium* may be facilitated by riboflavin (Luo et al., 2023). Similarly, all *OPB41* MAGs possessed genes for *cytochrome C* biosynthesis (*ccmA-F*), indicating a potential role in extracellular electron transport (Giangeri et al., 2023) (Fig. 6).

4. Discussion

4.1. Biomineralization of ferrihydrite in acidic peat soil

The comparable amounts of Fe extracted by HCl-Hydroxylamine and CBD suggest that crystalline Fe phases, including magnetite, did not form during ferrihydrite biomineralization (Fig. 3). The majority of Fe (II) species formed were likely re-adsorbed onto or precipitated within peat soils. The Fe K-edge X-ray absorption spectroscopic analysis revealed that Fe(III)/Fe(II) species primarily formed coordination complexes with functional groups of organic matter (Bhattacharyya et al., 2018). This complexation likely inhibits the transformation of ferrihydrite into more crystalline minerals (Piepenbrock et al., 2011; Shimizu et al., 2013). The absence of crystalline transformations in peatlands is in contrast to observations in relatively low-organic carbon terrestrial environments, such as paddy soils (Zhuang et al., 2015), aquifer or marine sediments (Sun et al., 2016; Lin et al., 2021), where magnetite formation is commonly reported. Secondarily formed magnetite can function as a semiconductor, facilitating the direct electron transfer between Fe(III) reducers (e.g. *Geobacter* and *Clostridium*) and methanogens (e.g. *Methanosarcina*), thus accelerating CH_4 formation (Zhuang et al., 2015; Zhao et al., 2020; Giangeri et al., 2023). However, our findings do not support this mechanism as a driver for enhanced CH_4 emissions in peatlands.

4.2. Fermentative ferrihydrite reduction enhances organic matter decomposition in acidic peat soil

4.2.1. Domination of fermentative ferrihydrite reduction

The low relative abundance of *Geobacteraceae* in our microcosms implies that respiratory Fe(III) reduction was not a dominant pathway for ferrihydrite reduction (Figs. 4 and 5). In contrast, members of *Clostridium*, known to perform fermentative Fe(III) reduction were significantly enriched in the presence of ferrihydrite (Dobbin et al., 1999; List et al., 2019). Additionally, the enriched *OPB41* sp. in the Fh treatment were phylogenetically related to *Coriobacteriaceae bacterium strain Es71-Z0120*, which is capable of Fe(III) reduction using H_2 as an electron source (Khomyakova et al., 2022). Genes encoding cytochrome C biosynthesis (*ccmA-F*) were identified in the enriched *OPB41* MAGs, supporting their role in exocellular electron transfer (Giangeri et al., 2023). The dominance of fermentative Fe(III) reducers is further supported by several other lines of evidence, including faster net H_2 consumption and greater amount of acetate accumulation (Figs. 1D and 2a), and a lack of significant change in net CO_2 formation in pre-methanogenic stage (Fig. 1B). The dominance of fermentative Fe(III)

reduction was also previously reported in other acidic peatlands (Reiche et al., 2008; Patzner et al., 2020), indicating that fermentative Fe(III) reduction could be widespread in this ecosystem.

4.2.2. Promotion of organic matter decomposition by fermentative ferrihydrite reduction

Ferrihydrite addition resulted in higher concentrations of DOC and acetate at the end of pre-methanogenic stage (Fig. 2a). During the subsequent methanogenic stage, the net formation of CO_2 and CH_4 increased in the Fh treatment (Fig. 1AB). Moreover, ferrihydrite stimulated the enrichment of several largely uncultured microbial groups, including *Sumerlaeaceae*, *Prolixibacteraceae* and *Bathyarchaeia* MAGs, which are potentially involved in degrading complex carbohydrates (e.g. cellulose, chitin and other polysaccharide) and in acetogenesis (Wang et al., 2024). These findings imply that ferrihydrite reduction facilitates the organic matter decomposition. Fueling of organic matter decomposition by Fe(III) reduction has also been reported in other anoxic soils, such as river sediments (Pallud et al., 2020; Aeppli et al., 2022; Reed et al., 2023), where Fe(III) was proposed to serve as an alternative terminal electron acceptor supporting anaerobic microbial respiration. Unlike respiratory Fe(III) reduction, which serves as an energy source, we propose that fermentative Fe(III) reduction enhances organic matter decomposition in acidic peat soils through two key mechanisms (Fig. 7): (1) Electron consumption via fermentative Fe(III) reduction helps alleviate the accumulation of reducing equivalents, making organic matter hydrolysis and fermenting process more thermodynamically favorable (Lovley et al., 2004). This mechanism is particularly active in pre-methanogenic phase; (2) In acidic peat soils, low pH suppresses organic matter decomposition (Vanlentine et al., 1994; Ye et al., 2012). Ferrihydrite reduction counteracts this effect by consuming H^+, thereby raising the pH toward neutral levels (Dong et al., 2017). The legacy effect of pH continues to promote faster organic matter decomposition during the methanogenic phase. Buffering acidity by Fe(III) reduction can be common in field sites, as a negative correlation between porewater Fe concentration and pH is also observed in porewater of Changbai peatlands (Wang et al., 2024), and other peatlands (Klüsel et al., 2008; Wagner et al., 2017). While both the Fh and Fh+AQDS treatments exhibited higher pH levels compared to the Control, more pronounced organic matter decomposition observed in the Fh+AQDS treatment may be partly attributed to greater thermodynamic favorability, particularly in DT. Collectively, two factors mentioned above both trigger a cascade effect in accelerating organic matter decomposition. Future studies should include more detailed experiments to disentangle relative contributions of these two factors.

4.3. Mechanisms of ferrihydrite reduction to facilitate methanogenesis

Our results indicate that ferrihydrite reduction facilitates methanogenesis despite an overall decrease in *mcrA* gene abundance (Fig. 4C). A similar trend was reported by Voggenreiter et al. (2025b), who found that Fe(III) reduction did not significantly affect net CH_4 formation in permafrost bogs, despite a notable decline in *mcrA* gene abundance. Isotopic fractionation ratios of CO_2 and CH_4 in DT peat soil suggest a predominance of acetoclastic methanogenesis, even though the methanogenic community was primarily composed of hydrogenotrophic methanogens (Fig. 2b). This apparent discrepancy could be explained by functional redundancy among methanogenic taxa in peatlands (Andersen et al., 2013; Wagner et al., 2017; Wang et al., 2024).

Electron budget calculations showed that fermentative ferrihydrite reduction in DT peat soil consumed 200 μmol of electrons per gram of peat in ferrihydrite-amended treatment. Consumption of H_2 by ferrihydrite reducers likely contributed to a notable decrease in the relative abundance of hydrogenotrophic *Methanobacterium*. Furthermore, outcompeting H_2 by fermentative Fe reducers contributed substantially to the lag phase of methanogenesis. At the same time, anaerobic respiration involving other electron acceptors in peat soils, such as quinones in specific organic matter, may also act as a redox buffer and outcompete methanogenesis (Peng et al., 2018; Gao et al., 2018; Guth et al., 2023). This is evidenced by the lag-phase observed in Control without ferrihydrite addition (Fig. 1A).

In contrast to H_2 consumption, fermentative ferrihydrite reduction does not use acetate in pre-methanogenic stage. Instead, as previously discussed, the enhanced organic matter decomposition both in pre-methanogenic and methanogenic phase provides additional substrates that support methanogenesis, especially the acetoclastic pathway. This is also evidenced by syntrophy between acetogens and methanogens. Moreover, a legacy of elevated pH during the pre-methanogenic stage may have further facilitated the rapid onset and enhancement of methanogenesis. Acetoclastic methanogenesis is generally more sensitive to pH than the hydrogenotrophic pathway, exhibiting optimal

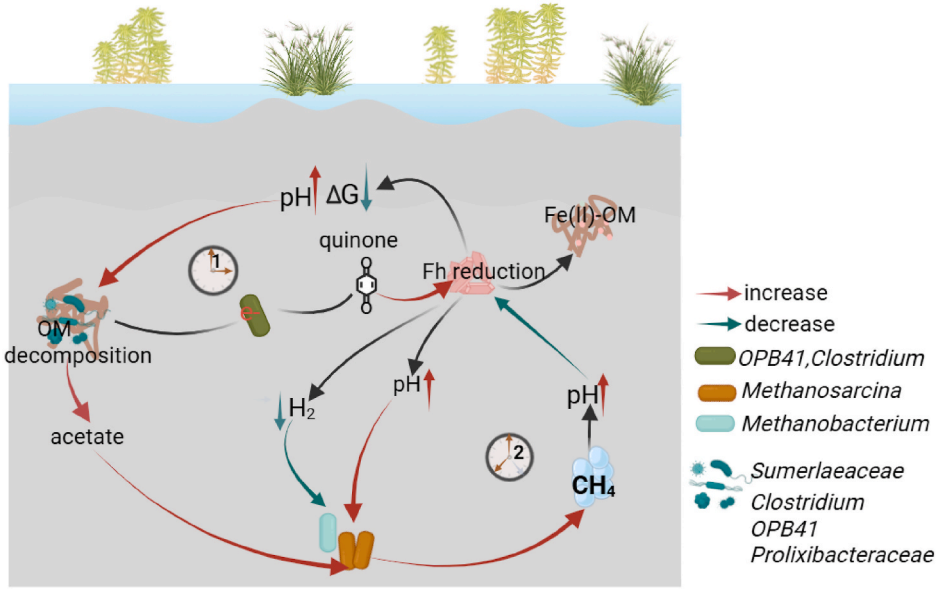

Fig. 7. Conceptual model of ferrihydrite reduction pathways that enhance organic matter decomposition and facilitate methanogenesis in acidic peatlands. Fh: ferrihydrite; OM: organic matter; △G: Gibbs free energy; Fe(II)-OM: complexes or precipitates between Fe(II) and organic matter.

activity around pH 5.5 (Kotsyurbenko et al., 2007; Ye et al., 2012). In acidic peat soils (pH < 5.0), ferrihydrite reduction raises the pH, thereby accelerating methanogenesis. This enhancement is supported by the more rapid net acetate consumption observed in ferrihydrite-amended treatments (Fig. 2a). Consistently, the *Methanosarcina* known for acetoclastic methanogenesis, showed an increase (Fig. 5c).

Ferrihydrite reduction was much slower or stopped in the methanogenic phase (Fig. 1C). This shift may reflect a thermodynamic tradeoff, where elevated pH levels resulting from active methanogenesis make ferrihydrite reduction less favorable (Bethke et al., 2011; Marquart et al., 2019). In contrast, when BES was added and methanogenesis was suppressed, the decreased pH rendered ferrihydrite to reduce again (Fig. 1C). A slight overlap between ferrihydrite reduction and methanogenesis has been also observed in previous studies, which is likely resulted from thermodynamic balance or microenvironmental heterogeneity (Reiche et al., 2008; Yang et al., 2016; Marquart et al., 2019).

Overall, our findings suggest that ferrihydrite addition stimulates methanogenesis, a process summarized in the conceptual model presented in Fig. 7. Firstly, fermentative Fe reduction enhances organic matter decomposition during the pre-methanogenic stage by alleviating thermodynamic constraints and increasing pH. The elevated pH as a legacy of ferrihydrite reduction continues to promote organic matter decomposition during the methanogenic stage, generating additional substrates that support acetoclastic methanogenesis in particular. Moreover, this sustained high pH enhances the activity of acetoclastic methanogens to further accelerate methanogenesis. The overall stimulating effect of ferrihydrite reduction on methanogenesis likely depends on the substrate quality (Sulman et al., 2022). In organic carbon-rich peat soils, substrate consumption by fermentative Fe reduction is minimal, and can be outweighed by its stimulating effect on methanogenesis. In surface and subsurface peatlands that undergo frequent redox oscillations, such as alternating dry-wet events (e.g. inundation after drought) and rhizosphere dynamics (Agethen et al., 2018), ferric phases can be replenished through the reoxidation of ferrous iron. Thus, interactions between Fe(III) reduction and methanogenesis proposed here are likely widespread in natural peatland environments.

5. Conclusions

This study investigates the influence of microbial ferrihydrite reduction on net CH_4 formation in acidic peat soils. Our findings suggest that fermentative Fe(III) reduction likely predominates in acidic peatlands. During the pre-methanogenic stage, this process promotes organic matter decomposition by enhancing the thermodynamic favorability of fermentation and increasing the pH. In the methanogenic stage, the legacy of elevated pH not only provides additional substrates for methanogenesis but also stimulates acetoclastic methanogen activity. In natural peatlands, Fe(III) species can regenerate at redox interfaces, enabling recurrent ferrihydrite reduction and sustained stimulation of methanogenesis. This mechanism may become increasingly relevant under ongoing climate change, as more intense rainfall events followed by prolonged drought periods are expected. Collectively, these findings underscore the importance of incorporating Fe-mediated pathways into peatland biogeochemical models to improve predictions of CH_4 emissions.

CRediT authorship contribution statement

Hong-Yan Wang: Writing – original draft, Software, Methodology, Investigation, Funding acquisition, Data curation, Conceptualization. **Xin-Yi Hu:** Investigation, Data curation. **Feng-Wu Zhou:** Writing – review & editing, Investigation. **Julio-Castillo Hernandez:** Writing – review & editing, Investigation. **Zhi-Guo Yu:** Writing – review & editing, Supervision, Funding acquisition. **Maxim Dorodnikov:** Writing – review & editing. **Klaus-Holger Knorr:** Writing – review & editing. **Andreas Kappler:** Writing – review & editing.

Declaration of competing interest

The authors declare that they have no known competing financial interests or personal relationships that could have appeared to influence the work reported in this paper.

Acknowledgments

We thank for Dr. Yixin He, and Dr. Yanyu Yue for collecting peat soils. We further acknowledge the financial support from Natural Science Foundation of China (NSFC) (Award No. 42207268 and 32471702) and National Science Foundation of Jiangsu province (Award No. BK20220454).

Appendix A. Supplementary data

Supplementary data to this article can be found online at https://doi.org/10.1016/j.soilbio.2025.110068.

References

Aeppli, M., Thompson, A., Dewey, C., Fendorf, S., 2022. Redox properties of solid phase electron acceptors affect anaerobic microbial respiration under oxygen-limited conditions in floodplain soils. Environmental Science and Technology 56, 17462–17470.
Agethen, S., Sander, M., Waldemer, C., Knorr, H.K., 2018. Plant rhizosphere oxidation reduces methane production and emission in rewetted peatlands. Soil Biology and Biochemistry 125, 125–135.
Andersen, R., Chapman, S.J., Artz, R.R.E., 2013. Microbial communities in natural and disturbed peatlands: a review. Soil Biology and Biochemistry 57, 979–994.
Aromokeye, D.A., Oni, O.E., Tebben, J., Yin, X., Richter-Heitmann, T., Wendt, J., Nimzyk, R., Littmann, S., Tienken, D., Kulkarni, A.C., Henkel, S., Hinrichs, K.U., Elvert, M., Harder, T., Kasten, S., Friedrich, M.W., 2021. Crystalline iron oxides stimulate methanogenic benzoate degradation in marine sediment-derived enrichment cultures. ISME Journal 15, 965–980.
Aramaki, T., Blanc-Mathieu, R., Endo, H., Ohkubo, K., Kanehisa, M., Goto, S., Ogata, H., 2020. KofamKOALA: KEGG Ortholog assignment based on profile HMM and adaptive score threshold. Bioinformatics 36, 2251–2252.
Bethke, C.M., Sanford, R.A., Kirk, M.F., Jin, Q., Flynn, T.M., 2011. The thermodynamic ladder in geomicrobiology. American Journal of Science 311, 183–210.
Bhattacharyya, A., Schmidt, M.P., Stavitski, E., Martínez, C.E., 2018. Iron speciation in peats: chemical and spectroscopic evidence for the co-occurrence of ferric and ferrous iron in organic complexes and mineral precipitates. Organic Geochemistry 115, 124–137.
Bräuer, S.L., Basiliko, N., Siljanen, H.M.P., Zinder, S.H., 2020. Methanogenic archaea in peatlands. FEMS Microbiology Letters 367, 1–17.
Bray, M.S., Wu, J., Reed, B.C., Kretz, C.B., Belli, K.M., Simister, R.L., Henny, C., Stewart, F.J., Dichistina, T.J., Branders, J.A., Fowle, D.A., Crowe, S.A., Glass, J.B., 2017. Shifting microbial communities sustain multiyear iron reduction and methanogenesis in ferruginous sediment incubations. Geobiology 15 (5), 678–689.
Callahan, B.J., Mcmurdie, P.J., Rosen, M.J., Han, A.W., Johnson, A.J.A., Holmes, S.P., 2016. DADA2: high-resolution sample inference from Illumina amplicon data. Nature Methods 13, 581.
Chen, Y.H., Prinn, R.G., 2006. Estimation of atmospheric methane emissions between 1996 and 2001 using a three-dimensional global chemical transport model. Journal of Geophysical Research Atmospheres 111, 1–25.
Chen, S., 2023. Ultrafast one-pass FASTQ data preprocessing, quality control, and deduplication using fastp. iMeta 2 (2), e107.
Chin, Y.P., Alken, G., O'Loughlin, E., 1994. Molecular weight, polydispersity, and spectroscopic properties of aquatic humic substances. Environmental Science and Technology 28, 1853–1858.
Conrad, R., 2005. Quantification of methanogenic pathways using stable carbon isotopic signatures: a review and a proposal. Organic Geochemistry 36, 739–752.
Conrad, R., 2020. Importance of hydrogenotrophic, aceticlastic and methylotrophic methanogenesis for methane production in terrestrial, aquatic and other anoxic environments: a mini review. Pedosphere 30, 25–39.
Coward, E.K., Thompson, A.T., Plante, A.F., 2017. Iron-mediated mineralogical control of organic matter accumulation in tropical soils. Geoderma 306, 206–216.
Cui, S., Liu, P., Guo, H., Nielsen, C.K., Pullens, J.W.M., Chen, Q., Pugliese, L., Wu, S., 2024. Wetland hydrological dynamics and methane emissions. Communications Earth & Environment 5, 1–17.
De Jong, A.E.E., Guererro-Cruz, S., van Diggelen, J.M.H., Vaksmaa, A., Lamers, L.P.M., Jetten, M.S.M., Smolders, A.J.P., Rasigraf, O., 2020. Changes in microbial community composition, activity, and greenhouse gas production upon inundation of drained iron-rich peat soils. Soil Biology and Biochemistry 149, 107862.
Dobbin, P.S., Carter, J.P., Juan, C.G.S.S., Von Höbe, M., Powell, A.K., Richardson, D.J., 1999. Dissimilatory Fe(III) reduction by Clostridium beijerinckii isolated from

freshwater sediment using Fe(III) maltol enrichment. FEMS Microbiology Letters 176, 131–138.
Dong, Y., Sanford, R.A., Chang, Y.J., McInerney, M.J., Fouke, B.W., 2017. Hematite reduction buffers acid generation and enhances nutrient uptake by a fermentative iron reducing bacterium, Orenia metallireducens Strain Z6. Environmental Science and Technology 51, 232–242.
Drake, H.L., Horn, M.A., Wüst, P.K., 2009. Intermediary ecosystem metabolism as a main driver of methanogenesis in acidic wetland soil. Environmental Microbiology Reports 1, 307–318.
Fletcher, S.E., Tans, P.P., Bruhwiler, L.M., Miller, J.B., Heimann, M., 2004. CH_4 sources estimated from atmospheric observations of CH_4 and its 13C/12C isotopic ratios: 2. Inverse modeling of CH_4 fluxes from geographical regions. Global Biogeochemical Cycles 18, 1–15.
Gao, C.Y., Sander, M., Agethen, S., Knorr, H.K., 2018. Electron accepting capability of dissolved and particulate organic matter control CO_2 and CH_4 formation in peat soils. Geochimica et Cosmochimica Acta 245, 266–277.
Giangeri, G., Tsapekos, P., Gaspari, M., Isfahani, P., Hong Lin, M.K.T., Treu, L., Kougias, P., Campanaro, S., Angelidaki, I., et al., 2023. Conductive materials alter the metabolic interaction between methanogens and sulfate-reducing bacteria. Environmental Science & Technology 16399–16413.
Guth, P., Gao, C.Y., Knorr, H.K., 2023. Electron accepting capabilities of a wide variety of peat materials from around the globe similarly explain CO_2 and CH_4 formation. Global Biogeochemical Cycles 37, 1–20.
Hyatt, D., Locascio, P.F., Hauser, L.J., Uberbacher, E.C., 2012. Gene and translation initiation site prediction in metagenomic sequences. Bioinformatics 28, 2223–2230.
Jones, A.M., Collins, R.N., Waite, T.D., 2017. Redox characterization of the Fe(II)-catalyzed transformation of ferrihydrite to goethite. Geochimica et Cosmochimica Acta 218, 257–272.
Khomyakova, M.A., Zavarzina, D.G., Merkel, A.Y., Klyukina, A.A., Pikhtereva, V.A., Gavrilov, S.N., Slobodkin, A.I., 2022. The first cultivated representatives of the actinobacterial lineage OPB41 isolated from subsurface environments constitute a novel order Anaerosomatales. Frontiers in Microbiology 13, 1–16.
Klüsel, K., Blöthe, M., Schlulz, D., Reiche, M., Drake, H.L., 2008. Microbial reduction of iron and porewater biogeochemistry in acidic peatlands. Biogeosciences 5, 1537–1549.
Knorr, K.H., Lischeid, G., Blodau, C., 2009. Dynamics of redox processes in a minerotrophic fen exposed to a water table manipulation. Geoderma 153, 379–392.
Knorr, K.H., Blodau, C., 2009. Impact of experimental drought and rewetting on redox transformations and methanogenesis in mesocosms of a northern fen soil. Soil Biology and Biochemistry 41, 1187–1198.
Kotsyurbenko, O.R., Friedrich, M.W., Simankova, M.V., Nozhevnikova, A.N., Golyshin, P. N., Timmis, K.N., Conrad, R., 2007. Shift from acetoclastic to H2-dependent methanogenesis in a West Siberian peat bog at low pH values and isolation of an acidophilic Methanobacterium strain. Applied and Environmental Microbiology 73, 2344–2348.
Lehours, A.C., Rabiet, M., Morel-Desrosiers, N., Morel, J.P., Jouve, L., Arbeille, B., Mailhot, G., Fonty, G., 2010. Ferric iron reduction by fermentative strain BS2 isolated from an iron-rich anoxic environment (Lake Pavin, France). Geomicrobiology Journal 27, 714–722.
Lin, B., Westerhoff, H.V., Röling, W.F.M., 2009. How Geobacteraceae may dominate subsurface biodegradation: physiology of Geobacter metallireducens in slow-growth habitat-simulating retentostats. Environmental Microbiology 11, 2425–2433.
Lin, X., Tfaily, M.M., Steinweg, J.M., Chanton, P., Esson, K., Yang, Z.K., Chanton, J.P., Cooper, W., Schadt, C.W., Kostka, J.E., 2014. Microbial community stratification linked to utilization of carbohydrates and phosphorus limitation in a Boreal Peatland at Marcell Experimental Forest, Minnesota, USA. Applied and Environmental Microbiology 80, 3518–3530.
Lin, Z., Sun, X., Roberts, A.P., Strauss, H., Lu, Y., Yang, X., Gong, J., Li, G., Brunner, B., Peckmann, J., 2021. A novel authigenic magnetite source for sedimentary magnetization. Geology 49, 360–365.
Liu, L., Chen, H., Jiang, L., Zhan, W., Hu, J., He, Y., Key, C.A.S., Ecological, M., Utilization, B., Restoration, E., Conservation, B., 2019. Response of anaerobic mineralization of different depths peat carbon to warming on Zoige plateau. Geoderma 337, 1218–1226.
List, C., Hosseini, Z., Lederballe Meibom, K., Hatzimanikatis, V., Bernier-Latmani, R., 2019. Impact of iron reduction on the metabolism of Clostridium acetobutylicum. Environmental Microbiology 21, 3548–3563.
Lovley, D.R., Holmes, D.E., Nevin, K.P., 2004. Dissimilatory Fe(III) and Mn(IV) reduction. Advances in Microbial Physiology 49, 219–286.
Lovley, D.R., Coates, J.D., Blunt-Harris, E.J., Woodward, J.C., 1996. Humic substances as electron acceptors for microbial respiration. Nature 382, 445–448.
Luo, D., Yu, H., Li, Y., Yu, Y., Chapman, S.J., Yao, H., 2023. A joint role of iron oxide and temperature for methane production and methanogenic community in paddy soils. Geoderma 433, 116462.
Marquart, K.A., Haller, B.R., Paper, J.M., Flynn, T.M., Boyanov, M.I., Shodunke, G., Gura, C., Jin, Q., Kirk, M.F., 2019. Influence of pH on the balance between methanogenesis and iron reduction. Geobiology 17, 185–198.
Nevin, K.P., Lovley, D.R., 2002. Mechanisms for accessing insoluble Fe(III) oxide during dissimilatory Fe(III) reduction by Geothrix fermentans. Applied and Environmental Microbiology 68, 2294–2299.
Pallud, C., Rhoades, C.C., Schneider, L., Dwivedi, P., Borch, T., 2020. Temperature-induced iron (III) reduction results in decreased dissolved organic carbon export in subalpine wetland soils, Colorado, USA. Geochimica et Cosmochimica Acta 280, 148–160.
Patro, R., Duggal, G., Love, M.I., Irizarry, R.A., Kingsford, C., 2017. Salmon provides fast and bias-aware quantification of transcript expression. Nature Methods 14, 417–419.
Patzner, S.M., Muller, W.C., Malusova, M., Baur, M., Nikeleit, V., Scholten, T., Hoeschen, C., Bryne, M.J., Borch, T., Kappler, A., Bryce, C., 2020. Iron mineral dissoluion releases iron and associated organic carbon during permafrost thaw. Nature Communications 11, 6329.
Peng, J.J., Wegner, C.E., Bei, Q.C., Liu, P.F., Liesack, W., 2018. Metatranscriptomics reveals a differential temperature effect on the structural and functional organization of the anerobic food web in rice field soil. Microbiome 6, 1–16.
Piepenbrock, A., Dippon, U., Porsch, K., Appel, E., Kappler, A., 2011. Dependence of microbial magnetite formation on humic substance and ferrihydrite concentrations. Geochimica et Cosmochimica Acta 75, 6844–6858.
Pruitt, K.D., Tatusova, T., Brown, G.R., Maglott, D.R., 2012. NCBI Reference Sequences (RefSeq): current status, new features and genome annotation policy. Nucleic Acids Research 40, 130–135.
Reiche, M., Torburg, G., Küsel, K., 2008. Competition of Fe(III) reduction and methanogenesis in an acidic fen. FEMS Microbiology Ecology 65, 88–101.
Reed, C.C., Dunham-Cheatham, S.M., Castle, S.C., Vuono, D.C., Sullivan, B.W., 2023. The contribution of Fe(III) reduction to soil carbon mineralization in Montane Meadows depends on soil chemistry, not parent material or microbial community. Journal of Geophysical Research: Biogeosciences 128, 1–14.
Riley, J.L., Michaud, L., 1994. Ontario Peatland Inventory: Field-Work Methods. Ontario Geological Survey, Toronto, Canada. Miscellaneous Paper.
Schwertmann, U., Cornell, R.M., 2000. Iron Oxides in the Laboratory: Preparation and Characterization. Wiley-VCH, Weinheim.
Seemann, T., 2014. Prokka: rapid prokaryotic genome annotation. Bioinformatics 30, 2068–2069.
Song, Y., Liu, C., Song, C., Wang, X., Ma, X., Gao, J., Gao, S., Wang, L., 2021. Linking soil organic carbon mineralization with soil microbial and substrate properties under warming in permafrost peatlands of Northeastern China. Catena 203, 105348.
Shimizu, M., Zhou, J., Schröder, C., Obst, M., Kappler, A., Borch, T., 2013. Dissimilatory reduction and transformation of ferrihydrite-humic acid coprecipitates. Environmental Science and Technology 47, 13375–13384.
Strack, M., Waddington, J.M., Tuittila, E.S., 2004. Effect of water table drawdown on northern peatland methane dynamics: implications for climate change. Global Biogeochemical Cycles 18, 1–7.
Stumm, W., Morgan, J.J., 1996. Aquatic chemistry — chemical equilibria and rates in natural waters. Environmental Science and Technology. Wiley-Interscience, New York.
Sulman, B.N., Yuan, F., O'Meara, T., Gu, B., Herndon, E.M., Zheng, J., Thornton, P.E., Graham, D.E., 2022. Simulated hydrological dynamics and coupled iron redox cycling impact methane production in an Arctic soil. Journal of Geophysical Research: Biogeosciences 127, 1–14.
Sun, J., Chillrud, S.N., Mailloux, B.J., Bostick, B.C., 2016. In situ magnetite formation and long-term arsenic immobilization under advective flow conditions. Environmental Science and Technology 50, 10162–10171.
Thauer, R.K., Kaster, A.K., Seedorf, H., Buckel, W., Hedderich, R., 2008. Methanogenic archaea: ecologically relevant differences in energy conservation. Nature Reviews Microbiology 6, 579–591.
Uritskiy, G.V., DiRuggiero, J., Taylor, J., 2018. MetaWRAP—a flexible pipeline for genome-resolved metagenomic data analysis. Microbiome 6, 1–13.
Vanlentine, D.W., Holland, E.A., Schimel, D.S., 1994. Ecosystem and physiological controls over methane production in northern wetlands. Journal of Geophysical Research: Atmosphere 99, 1563–1571.
Vigderovich, H., Liang, L., Herut, B., Wang, F., Wurgaft, E., Rubin-Blum, M., Sivan, O., 2019. Evidence for microbial iron reduction in the methanic sediments of the oligotrophic southeastern Mediterranean continental shelf. Biogeosciences 16, 3165–3181.
Viollier, E., Inglett, P.W., Hunter, K., Roychoudhury, A.N., Van Cappellen, P., 2000. The ferrozine method revisited: fe (II)/Fe (III) determination in natural waters. Applied Geochemistry 15, 785–790.
Voggenreiter, E., ThomasArrigo, L., Bottaro, M., Kilian, J., Straub, D., Ring-Hrubesh, F., Bryce, C., Stahl, M., Kappler, A., Joshi, P., 2025a. Suppression of methanogenesis by microbial reduction of iron-organic carbon associations in fully thawed permafrost soil. Journal of Geophysical Research: Biogeosciences 130.
Voggenreiter, Eva, ThomasArrigo, L., Kilian, J., Straub, D., Friedel, M., Stahl, M., Kappler, A., Joshi, P., 2025b. Reduction of iron-organic carbon associations shifts net greenhouse gas release after initial permafrost thaw. Soil Biology and Biochemistry 203, 109735.
Wagner, R., Zona, D., Oechel, W., Lipson, D., 2017. Microbial community structure and soil pH correspond to methane production in Arctic Alaska soils. Environmental Microbiology 19, 3398–3410.
Watmough, S., Gilbert-Parkes, S., Basiliko, N., Lamit, L.J., Lilleskov, E.A., Andersen, R., Yu, Z.G., Zahn, G., 2022. Variation in carbon and nitrogen concentrations among peatland categories at the global scale. PLoS One 17, 1–15.
Wang, H., Yu, Z., Zhou, F., Hernandez, J., Grandjean, A., Biester, H., Xiao, K., Knorr, K., 2024. Microbial communities and functions are structured by vertical geochemical zones in a northern peatland. Science of the Total Environment 950, 175273.
Wang, H.Y., Byrne, J.M., Perez, J.P.H., Thomas, A.N., Goettlicher, J., Hofer, H.E., Mayanna, S., Kontny, A., Kappler, A., Guo, H.M., Benning, L.G., Norra, S., 2020. Arsenic sequestration in pyrite and greigite in the buried peat of As-contaminated aquifers. Geochimica et Cosmochimica Acta 284, 107–119.
Wang, Y., Wang, H., He, J., Feng, X., 2017. Iron-mediated soil carbon response to water-table decline in an alpine wetland. Nature Communications 8, 1–9.
Weishaar, J.L., Aiken, G.R., Bergamaschi, B.A., Fram, M.S., Fujii, R., Mopper, K., 2003. Evaluation of specific ultraviolet absorbance as an indicator of the chemical composition and reactivity of dissolved organic carbon. Environmental Science and Technology 37, 4702–4708.

Whiticar, M.J., 1999. Carbon and hydrogen isotope systematics of bacterial formation and oxidation of methane. Chemical Geology 161, 291–314.
Yang, L., Steefel, C.I., Marcus, M.A., Bargar, J.R., 2010. Kinetics of Fe(II)-catalyzed transformation of 6-line ferrihydrite under anaerobic flow conditions. Environmental Science and Technology 44, 5469–5475.
Yang, Q., Li, X., Han, Z., Wang, X., Zhao, W., Yi, S., Lu, H., 2022. DCB dissolution of iron oxides in aeolian dust deposits controlled by particle size rather than mineral species. Scientific Reports 12, 1–15.
Yang, Z., Wullschleger, S.D., Liang, L., Graham, D.E., Gu, B., 2016. Effects of warming on the degradation and production of low-molecular-weight labile organic carbon in an Arctic tundra soil. Soil Biology and Biochemistry 95, 202–211.
Yang, Z., Sun, T., Kleindienst, S., Straub, D., Kretzschmar, R., Angenent, L.T., Kappler, A., 2021. A coupled function of biochar as geobattery and geoconductor leads to stimulation of microbial Fe(III) reduction and methanogenesis in a paddy soil enrichment culture. Soil Biology and Biochemistry 163, 108446.
Ye, R., Jin, Q., Bohannan, B., Keller, J.K., McAllister, S.A., Bridgham, S.D., 2012. pH controls over anaerobic carbon mineralization, the efficiency of methane production, and methanogenic pathways in peatlands across an ombrotrophic-minerotrophic gradient. Soil Biology and Biochemistry 54, 36–47.
Zhang, Y., Hao, Q., Wang, O., Zhang, X.H., Liu, F., 2023. Fermentative iron reduction buffers acidification and promotes microbial metabolism in marine sediments. Journal of Environmental Chemical Engineering 11, 110922.
Zhang, Y., Naafs, B.D.A., Huang, X., Song, Q., Xue, J., Wang, R., Zhao, M., Evershed, R.P., Pancost, R.D., Xie, S., 2022. Variations in wetland hydrology drive rapid changes in the microbial community, carbon metabolic activity, and greenhouse gas fluxes. Geochimica et Cosmochimica Acta 317, 269–285.
Zhang, L., Liu, X., Duddleston, K., Hines, M.E., 2020. The effects of pH, temperature, and humic-like substances on anaerobic carbon degradation and methanogenesis in ombrotrophic and minerotrophic Alaskan peatlands. Aquatic Geochemistry 26, 221–244.
Zhao, Z., Li, Y., Zhang, Y., Lovley, D.R., 2020. Sparking anaerobic digestion: promoting direct interspecies electron transfer to enhance methane production. iScience 23, 101794.
Zhuang, L., Xu, J.L., Tang, J., Zhou, S.G., 2015. Effect of ferrihydrite biomineralization on methanogenesis in an anaerobic incubation from paddy soil. Journal of Geophysical Research: Biogeosciences 120, 876–886.
Zhuang, Q., Melillo, J.M., Sarofim, M.C., Kicklighter, D.W., McGuire, A.D., Felzer, B.S., Sokolov, A., Prinn, R.G., Steudler, P.A., Hu, S., 2006. CO_2 and CH_4 exchanges between land ecosystems and the atmosphere in northern high latitudes over the 21st century. Geophysical Research Letters 33, 2–6.